Analysis of CdS/CdTe photovoltaic cells manufactured on polyimide substrates

T. POTLOG*
Department of Physics and Engineering, Moldova State University, MD 2009, Chisinau, Moldova

The development of CdS/CdTe solar cells on Upilex-S foils coated with a semitransparent indium tin oxide (ITO) is reviewed in this article. The basic manufacturing technique includes the chemical-bath deposited CdS and the close-spaced sublimated CdTe, the solution-$CdCl_2$ treatment, and an evaporated Ni contact. The devices have been investigated using the current-voltage *(I-U)* characteristics and the capacitance-voltage *(C-U)* measurements in order to define the transport mechanism in a photovoltaic device and the basic electronic parameters. ITO/CdS/CdTe photovoltaic cells with conversion efficiencies exceeding 4% have been developed on polyimide foils with the area of 1.7 cm^2. Both *I-U* and *C-U* characteristics of the poly/ITO/CdS/CdTe cell show the typical behavior of the two-diode model.

(Received September 26, 2013; accepted July 10, 2014)

Keywords: Polyimide, CdS, CdTe, Photovoltaic cell

1. Introduction

In order for the photovoltaic devices to become competitive with other forms of energy, conventional or alternative, they must primarily have a higher efficiency combined with as a lower manufacturing cost as possible. These requirements depend on the used materials, as well as on the manufacturing technologies of such devices. Lowering the cost of manufacturing photovoltaic cells using simple technology, cheaper substrates and materials is extremely important. The efficiency of laboratory samples of silicon cell based on p-n junctions exceeds 24%, a value close to the upper theoretical limit of the silicon-based solar cells. Thin film polycrystalline silicon cells require special substrates and are expensive. Present estimates show that the cost of silicon PV cannot continue declining much longer. Many analysts anticipate – and the initial results on the market seem to confirm these anticipations – that one or more of the thin-film technologies will lead the way in providing drastic cost reductions. These are: $CuInGaSe_2$ [1,2], CdTe [3-6], and amorphous silicon. [7].

Polycrystalline CdS/CdTe thin film solar cells are important for terrestrial applications because of their high efficiency, long term stable performance and potential for low cost production. The highest record efficiency of 16.5% has been achieved at NREL, USA [8]. Glass is the most commonly used substrate but recently some effort has been made to develop flexible solar cells on polyimide and metal foils. However, the advent of flexible solar cells in the recent years offers significant advantages over the conventional photovoltaic cells, especially in several application areas. Low weight and flexibility is particularly attractive due to: the possibility of low cost production using roll-to-roll manufacturing; it can be wrapped easier onto any suitable oriented or non concrete oriented roof surfaces; the mobility of the power source: for example, for water pumping and irrigation in distributed areas; for very high specific power (kW/kg, defined as ratio of electrical power output to the weight of the solar module) for space application. Lightweight and flexible CdS/CdTe solar cells manufactured by physical vapor deposition with the efficiency of ~ 11% have been developed by the ETHZ group [9, 10]. This paper presents the review of CdS/CdTe solar cells manufactured by chemical bath deposition and close space sublimation methods on high temperature resistant polyimide film substrates.

2. Method of preparation

The substrates used for the development of thin film layers were Upilex-S polyimide and Upilex-S polyimide/ITO foils coated with a semitransparent indium tin oxide (ITO) (SnO_2+In_2O_3) layer. The resistivity of ITO layers is ~3.5 Ω/□; the conductivity ~ 300 $\Omega^{-1}cm^{-1}$ (300 K) and the carrier concentration is aproximately $7 \cdot 10^{19}$ cm^{-3}. The CdS window layer was developed by chemical bath deposition (CBD) and the absorber layer CdTe was deposited on top of CdS by close-spaced sublimation (CSS). The choice of the CBD method was probably due to the fact that CBD makes a very compact CdS film that covers perfectly the TCO layer. The CdS thin films were deposited on polyimide and poly/ITO substrates from a chemical bath containing a water solution of $CdSO_4$ (1 mM), NH_4OH (0.2 M), $(NH_4)_2SO_4$ (0.03 M) and relative to Cd 0.001 at. % NH_4Cl. The pH of the solution was 10.7. When the solution reached 85 °C thiourea (10 mM) was added. $CdCl_2$ formation occurs during the introduction of NH_4Cl dopant in the deposition solution. The deposition process of the layer takes 30 min. CdS thickness 300 – 350 nm was achieved by a three times repeated deposition. The

details of the CBD deposition of the CdS can be found in [11]. 99.999 % pure CdTe was used. The CdTe thin films were deposited in a vacuum of about $2 \cdot 10^{-5}$ torr in the CSS system, where the source and the substrate are placed at a 2 cm distance from each other. The source and the substrate are heated to 590°C and (350-400)°C, respectively. The thickness of CdTe layers was about 6 μm. $CdCl_2$ treatment was performed at 400°C for 35 min to improve the quality of the CdTe layer. After the $CdCl_2$ treatment, a Ni electrode was prepared by thermal evaporation followed by heat treatment at 155°C for 15 min. For the investigation of the surface morphology a JEOL-type JSM 6400 F scanning electron microscope (SEM) were employed. X-ray diffraction was carried out on a Rigaku RU-200 XRD system using Cu $K_{\alpha 1}$/40 kV/40mA radiation source (λ=.54056 A), Ni filter. The X-ray diffraction (XRD) analysis was performed using Rigaku software PDXL. The optical transmission spectra were recorded using a JASCO V-670 spectrophotometer in the wavelength range of 300–1200 nm. The temperature-dependent dark *I–U* and *C–U* measurements of the samples were performed to a computer interfaced DLS-2000 system.

3. Results and discussions

3.1. Morphology of CBD-CdS films

.

Fig. 1 and Fig. 2 show the surface morphologies of CdS layer deposited on polyimide after deposition, before treatment and after heat treatment at T = 400°C in vacuum (~0.1 Pa) and H_2 atmosphere at normal pressure. From the surface morphologies it can be seen that only the homogeneous covering under the layer film is visible with some superficial grains that have not changed with a heat treatment temperature of up to 400 °C and treatment duration of up to 120 min. Cross-section images (Fig. 3) show that CdS layers grow in a columnar structure. From the cross-section it can be seen that the film thickness is 300-350 nm after three 30 min deposition time. The films are pinhole-free and exhibit a good adherence to the polyimide substrate. The_polycrystalline CdS films are formed by crystallites with the size of ~ 40 nm forming granules with the size of ~ 150 nm.

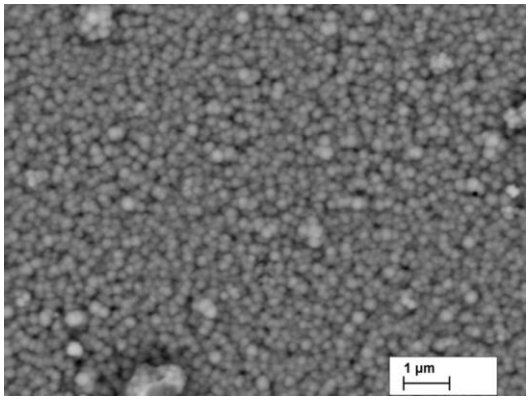

Fig. 1 . SEM image of the as-deposited CBD CdS thin films before treatment.

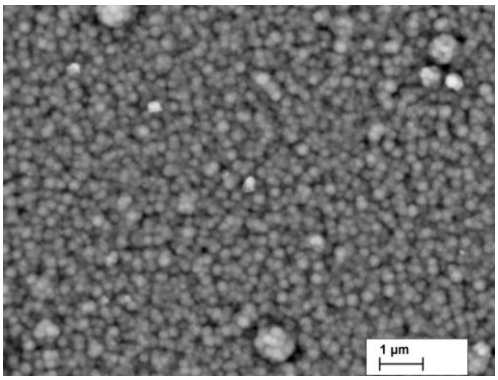

Fig. 2. SEM image of the CBD CdS thin films after treatment.

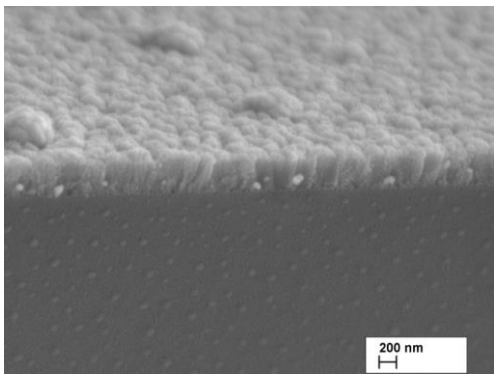

Fig. 3. Cross- section image of CBD CdS thin film after heat treatment.

3.2. Optical properties

In the Fig. 4 transmission measurements show that CdS layers deposited on polyimide substrate treated at different temperatures during 30 min have a high transparency in the visible region in comparison with the polyimide substrate, making them excellent window layers for solar cells applications.

Interference fringes are seen in these films. The transmittance values are taken as an average of maximum (or minimum) values of these fringes. From Fig.4 we can see that the transmittance of the layers deposited on polyimide varies between 70% - 90%. The transmission spectra of poly/ITO/CdS samples (Fig. 5) show average transmission ~ 65 %.

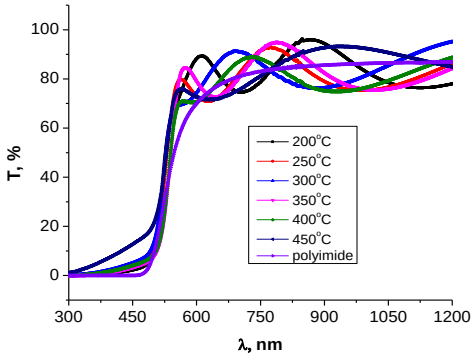

Fig. 4. Transmission spectra of CdS films treated at different temperatures.

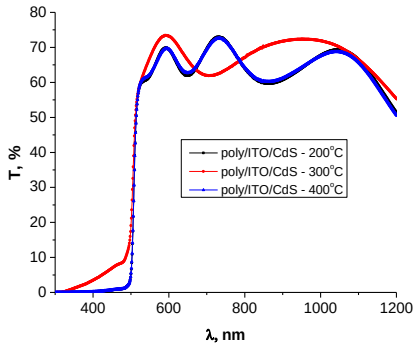

Fig. 5. Transmission spectra of poly/ITO/CdS at different temperatures.

3.3. Electrical properties

In order to estimate the sheet resistance and mobility of the films the method of four contacts was used. The Hall measurements in a constant magnetic field (magnetic induction B=0.24 T) and in a stabilized direct current (DC) were performed. Each sample for three different values of current (50 μA – 2 mA) was measured. Also, a measurement was made in a constant magnetic field and in a stabilized alternating current (AC) frequency - 930 Hz. The results are presented in Table 1. The CdS layers treated at the lowest temperatures have the highest mobility. The mobility decreases with the increase of the treatment temperature created. Annihilation of sulfur and cadmium vacancies creates two donor centers of Cl_s^+ and $(OH)_s^+$. These substitution impurities on the sulfur site behave as shallow donors contributing to the decrease of resistivity. The electron concentration of CdS thin films is 10^{19} cm^{-3}. The high concentration of electrons corresponds to the high density of shallow donors in CdS lattice.

Table 1. Results of Hall measurements for CdS layers annealed in hydrogen for 30 min.

Treatm. temperature, °C	Mobility, $cm^2/V{\cdot}s$		Resistivity $\times10^{-2}$, Ω·cm		Concentration $\times10^{19}$, cm^{-3}	
	DC	AC	DC	AC	DC	AC
200	9.3 ± 0.4	10.8	4.57± 0.01	4.64	1.5 ± 0.1	1.25
250	8.0 ± 0.7	6.55	2.40± 0.01	2.45	3.3 ± 0.3	3.9
300	3.5 ± 0.2	3.4	7.31± 0.03	7.50	2.46± 0.15	2.43
350	4.5 ± 0.2	5.8	7.22± 0.15	7.30	1.9 ± 0.1	1.48
400	4.5 ± 0.2	4.63	5.03± 0.02	5.05	2.76± 0.15	2.67

We assume that during the introduction in deposition solution of NH_4Cl dopant $CdCl_2$ formation occurs. The $CdCl_2$ incorporation in the process of deposition from a solution could be explained by the following equation [11]:

$$CdCl_2(solution) \xrightarrow{CdS} (V_{Cd}\,2Cl_S)^x + Cd_{Cd}{}^x$$

$$(1+n)(V_{Cd}\,2Cl_S)^x \xrightarrow{CdS} V_{Cd}^{2-} + 2ne^- + 2(1+n)Cl_S^+ + nS_{2g}\uparrow$$

The hydroxide and chloride ions on the sulfur site form $V_{Cd}2Cl_s$ and $V_{Cd}2(OH)_s$ electrically neutral defect complexes. The increase in the annealing temperature accelerates sintering of as deposited polycrystalline CdS and retention of larger quantities of chloride and hydroxide impurities, which would otherwise evaporate and decompose. Upon the decomposition of two hydroxide groups in CdS lattice one water molecule and one sulfur vacancy will be released.

3.4. Effect of chlorine doping on CSS - CdTe thin \ films

CdTe thin films were grown at the 320°C substrate temperature and the source temperature of 590°C. These source-substrate temperatures are the most suitable in preparing CdTe thin films for solar cell applications. Because the obtained CdTe layers have a high resistance (10^7-10^8) Ω and are not photosensitive, the necessity to activate them in a chemical solution and perform a heat treatment in the air appears. For the activation we used a saturated solution of cadmium chloride $CdCl_2$:CH_3OH [12]. Initially poly/ITO/CdS/CdTe structures were kept in such a solution and left for a while, and then heated in the air at different temperatures. The influence of the heat treatment duration on the lateral resistance of CdTe thin films kept in a saturated solution of $CdCl_2$ for 60 min is shown in Fig.6. If the CdTe layer is kept more than 2 hours in a saturated solution of $CdCl_2$ then it deteriorates.

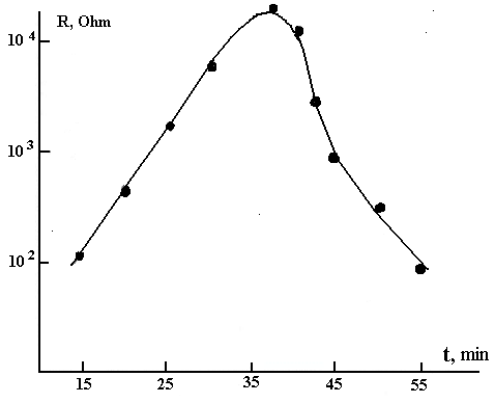

Fig. 6. The dependence of the lateral resistance of CdTe layers in function of duration of the treatment with time kept in the $CdCl_2$ saturation solution 60 minutes.

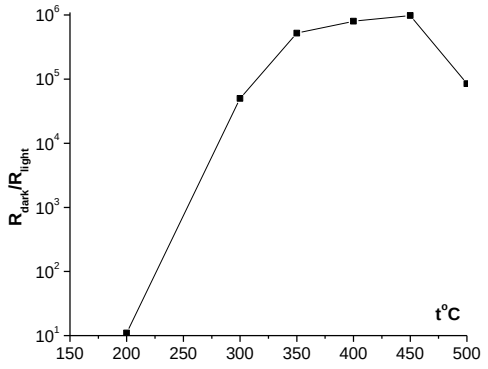

Fig. 7. Dependence of the relative sensitivity (R_d/R_{ill}) of CdTe layers in function of treatment temperature.

As one can see from Fig. 6 the optimal duration of heat treatment in the air is 35- 40 min. The investigation of the relative sensitivity of CdTe layer as a function of the treatment temperature (Fig. 7) with 60 min time staying in the $CdCl_2$ solution and 35 min duration of heat treatment allows us to see that with the increase of treatment temperature the relative sensitivity of CdTe layers increases and at $T_{tr} = 350^0$C-450°C is almost constant and reaches 10^6. Investigation of this dependence allowed us to determine the optimum photosensitivity temperature which was then used to manufacture poly/ITO/CdS/CdTe photovoltaic cells. SEM images and results of the EDX analysis of CdTe layers before and after the heat treatment in $CdCl_2$ are shown in Figs. 8 and 9. We note that both layers are composed of crystallites of different sizes. For the CdTe layer before treatment with $CdCl_2$ crystallites vary in the range of 1.5 -5 μm. After $CdCl_2$ chemical activation and thermal treatment in the air at 400°C ± 5°C crystallites vary from ~ 2 μm to ~ 8 μm. As we see the heat treatment does not change so much the size of the crystallite. After the heat treatment there is a stronger deviation from the stoichiometric composition in the direction of the Te excess increase. The presence of the graphite indicates his evaporation from the polyimide substrate.

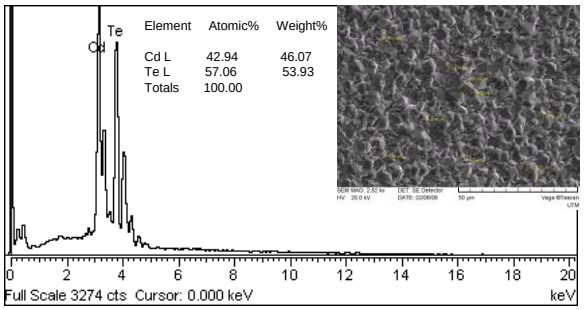

Fig. 8. SEM image and results of the EDX analysis of CdTe layers before chemical and heat treatment.

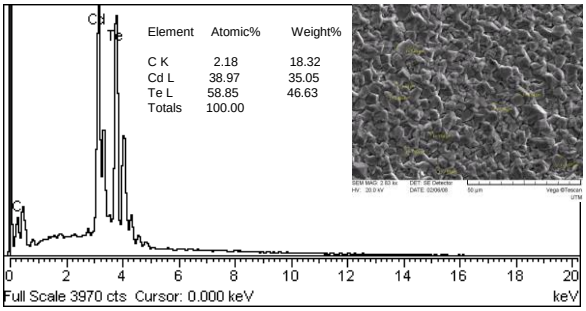

Fig. 9. SEM image and results of the EDX analysis of CdTe layers after chemical and heat treatment.

As a result of the thermal treatment the recrystalization process takes place and leads to crystallite size increase and orientation. The activation process occurs as a result of CdTe chemical treatment and leads to the introduction of active centers.

Also the CdTe layers before and after the chemical and thermal treatment were investigated using the X-ray diffraction method. The X-ray diffraction pattern of the CdTe layers before and after the $CdCl_2$ chemical and thermal treatment is shown in Fig. 10. The diffraction pattern of the CdTe layer before the chemical and heat treatment shows one diffraction maximum (111) corresponding to CdTe. The diffraction picture of the CdTe layer after the chemical and heat treatment indicates a set of diffraction peaks (111), (220), (311), (400) and (331) of different intensity. The intensity of the diffraction peak (111) present in the CdTe layer before the chemical and heat treatment decreases indicates a less perfect crystalline structure. The maximum noted with * in the XRD pattern corresponds to the polyimide substrate. The present plane (111) in both spectra indicates that the growth does not change the crystallite growth direction after the heat treatment. The lattice constant was calculated using the formula

$$a = d\sqrt{h^2 + k^2 + l^2} \qquad (1)$$

where *d* is the spacing between the planes in the atomic lattice determined by the formula

$$\frac{d_{nkl}}{n} = \frac{\lambda}{2\sin\theta} \quad (2)$$

where Θ is the incident angle, λ is the wavelength of the x-ray and n is an integer representing the order of the diffraction peak. The lattice constant is 6.481 Å and is in good agreement with the literature values [13]. Detailed phase analysis does not show the presence of $CdCl_2$ or other phases. All diffraction peaks correspond to CdTe phases with zincblend structure.

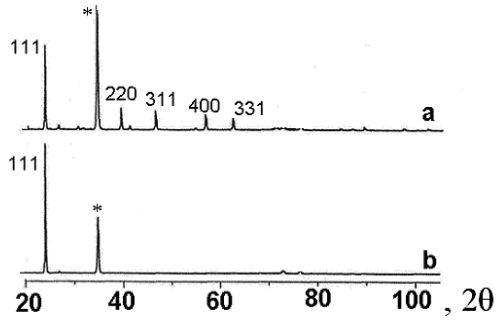

Fig. 10. The XRD pattern of the CdTe films deposited on poly/ITO/CdS substrates a – after chemical and heat treatment; b – before chemical and heat treatment.

3.5 Manufacturing ITO/CdS/CdTe photovoltaic cells

An ultralight flexible ITO/CdS/CdTe photovoltaic cell has been developed utilizing approximately 25-μm coated polyimide foils which have an excellent flexibility with high optical transparency as well as a thermal endurance of up to 420°C. A set of poly/ITO/CdS/CdTe photovoltaic cells was manufactured at the following substrate temperatures: 350°C; 370°C and 400°C. Depending on the substrate temperature of the CdTe layer the cells were marked as CS1 (T_s=350°C), CS2 (T_s = 370°C) and CS3 (T_s = 400°C). The source temperature was kept at 590°C. The effective area of the CdTe solar cells was 1.7 cm^2. The top view and the cross-section image of poly/ITO/CdS/CdTe are illustrated in Fig. 11 and Fig. 12, respectively.

3.6 Current-voltage characteristics of the poly/ITO/CdS/CdTe photovoltaic cells at illumination

Current-voltage characteristics of a set of three poly/ITO/CdS/CdTe solar cells have been studied at illumination through the polyimide. The current-voltage characteristics measured at 100 mW/cm^2, T = 300 K are shown in Fig. 13.

Fig. 11. Top view of the poly/ITO/CdS/CdTe photovoltaic cell.

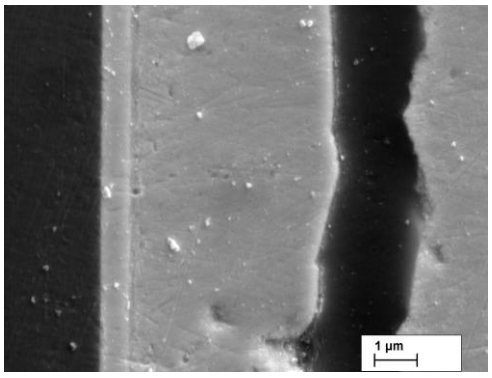

Fig. 12. Cross-section TEM image of the poly/ITO/CdS/CdTe photovoltaic cell.

At the illumination of the poly/ITO/CdS/CdTe solar cell the photons absorbed in the CdTe layer generate electron-hole pairs which are separated by the internal electric field of the junction and dissipate the photocurrent J_L. Because the direction of the photo-generated carriers is so that the photocurrent is opposite to the diffusion current of the forward biased diode, through the load resistance will flow the current

$$J=J_s(exp(eV/nkT-1)) - J_L \quad (3)$$

where J_s – saturation current density; k- Boltzmann's constant; n - ideality factor.

From these characteristics we determined the photovoltaic parameters: the short circuit current density J_{sc}, the open circuit voltage U_{oc}, the fill factor FF, the solar energy efficiency conversion into electrical energy η, the R_s series and the R_{sh} shunt resistances and presented them in Table 2. The photovoltaic parameters of the poly/ITO/CdS/CdTe/ cells depend on the substrate temperature of CdTe thin films. At the higher substrate deposition temperatures (large grains) of CdTe thin films the values of photovoltaic parameters are higher. The open circuit voltage U_{oc} is low due to the presence of a series resistance and a shunt resistance, which lead to the decrease of the maximum current J_m and the maximum voltage U_m, the fill factor, and the solar cell efficiency.

CS1 photovoltaic cell operates as "reach-through diode". The current-voltage curves from quadrant I for CS2 and CS3 have a non-ideal behavior, because of the most difficult problem, achieving stable ohmic contacts to cadmium telluride. The model of double Schottky diodes is used for the interpretation of this behavior. The fill factor losses of the solar cells can be due to back contact to CdTe which affect the fill factor. Also, the fill factor depends on the series/shunt resistance, the saturated dark current density and the ideality factor. As one can see from the table 2 the value of the series rezistance is higher for all cells and this is due probably to the fact that the cells used wet $CdCl_2$ treatment that may contain oxide on the surface of CdTe. So, the low value of the fill factor in the case of CS1 photovoltaic devices is due to higher series and to low shunt value resistances, but in the case of CS2 and CS3 cells it is caused by the high series resistance, as well as by the back contact properties. The open circuit voltage U_{oc} and the short circuit current density J_{sc} dependencies on the intensity of illumination of the poly/ITO/CdS/CdTe photovoltaic devices are shown in Fig. 14 and Fig. 15. For CS1 cell the open circuit voltage does not change with intensity of illumination because it operates in the "reach-through diode" regime. With the increase of light intensity, U_{oc} tends to saturation for CS2 and CS3 cells, and the short circuit current density for all the solar cells depends linearly on the intensity of illumination. This short circuit current density variation principle for all cells and for the open circuit voltage in the case of CS2 and CS3 is in good agreement with the abrupt heterojunction theory [14]. The open circuit voltage is obtained from equation (3), if we take J = 0 (for R = ∞).

Table 2. Photovoltaic parameters of photovoltaic cells with variable CdTe grain size.

Photovoltaic cells	**d, μm**	**J_{sc}, mA/cm^2**	**U_{oc}, V**	**FF, %**	**η, %**	**R_s, Ohm cm^2**	**R_{sh}, Ohm cm^2**
CS1	2.3	17.16	0.5	31.3	2.7	10.2	334
CS2	5.2	18.18	0,6	34.7	3.82	5.6	566
CS3	6.5	16.2	0.56	43.6	4.13	3.3	1000

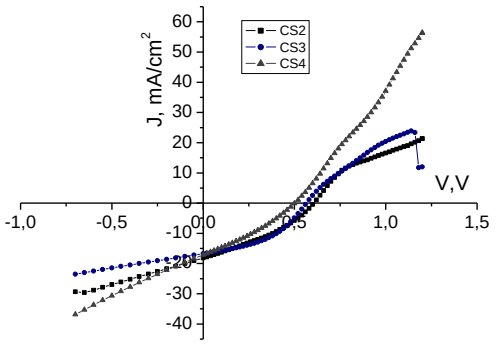

Fig. 13. J-V characteristics for ITO/poly/CdS/CdTe devices from films with variable CdTe grain size (different substrate temperatures) at 100 mW/cm^2 and 300 K.

$$U = U_{OC} = \frac{nKT}{e}\ln\left(\frac{J_{sc}}{J_L} + 1\right) \tag{4}$$

It seems that under short circuit condition (R = 0), U = 0 and from equation (4) the resulting photocurrent density is

$$J_L : J(U=0) = J_{sc} = J_L \tag{5}$$

Taking into consideration this and the fact that the short circuit current density depends linearly on the intensity of illumination J_{sc}=BE, the relation to the open-circuit voltage can be transcribed as:

$$U_{OC} = \frac{nKT}{e}\ln\frac{J_L}{J_{sc}} \tag{6}$$

At irradiation with an intense light beam the current density $J_L >> J_s$ and then

$$U_{OC} \approx 0{,}025\ln\frac{J_L}{J_{sc}} \tag{7}$$

Usually, in the case of heterojunction solar cells, the carrier concentration in the diffused layer is far greater than the carrier concentration in the "base" so that the saturation current J_s will be determined by the equation

$$J_s = qp_n\sqrt{\frac{D_p}{\tau_p}} \tag{8}$$

Using this relation and taking into consideration the expressions

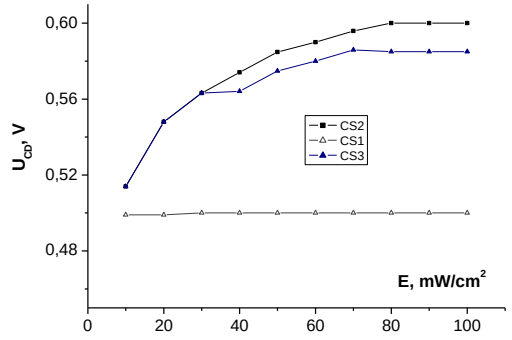

Fig. 14. The dependence of U_{oc}= f (E) from poly/ITO/ CdS/CdTe photovoltaic cells manufactured at different substrate temperatures.

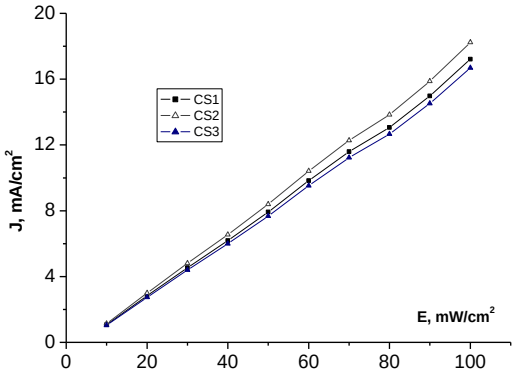

Fig. 15. The dependence of J_{sc}= f (E) from poly/ITO/ CdS/CdTe photovoltaic cells manufactured at different substrate temperatures.

$$n_i = 2\left(\frac{2\pi kT}{h^2}\right)^{\frac{3}{2}}(m_n^* m_p^*)^{\frac{3}{4}}\exp\left(-\frac{E_g}{2kT}\right) \quad (9)$$

$$p_n n_{ni} = n_i^2;\ n_n = \frac{1}{q\rho_n\mu_n} \quad (10)$$

For U_{oc} we can write

$$U_{OC} = 0{,}025\ln\left[\frac{J_L \exp\frac{E_g}{kT}}{4q^2\left(\frac{2\pi kT}{h^2}\right)^3 (m_n^{\bullet} m_p)^{\frac{3}{2}}\mu_n\rho_n\left(\frac{D_p}{\tau_p}\right)^{\frac{1}{2}}}\right] \quad (11)$$

It seems that to achieve the greatest possible value for U_{oc}, besides choosing a semiconductor with an optimum E_g it is necessary to have a low resistivity and a high value for the lifetime of nonequilibrium carriers.

3.7 Dark current-voltage characteristics of the poly/ITO/CdS/CdTe photovoltaic cells

The dark I–U current-voltage characteristics of a photovoltaic cell CS3 with the highest efficiency measured in the temperature interval ranging from 290 K to 370 K are shown in Fig. 16. With the increase in the measurement temperature both the forward and the reverse current increases. The rectification coefficient increases from 30 (290 K) to 100 (370 K). At room temperature the *I-U* curves show the typical behavior of the two-diode model.

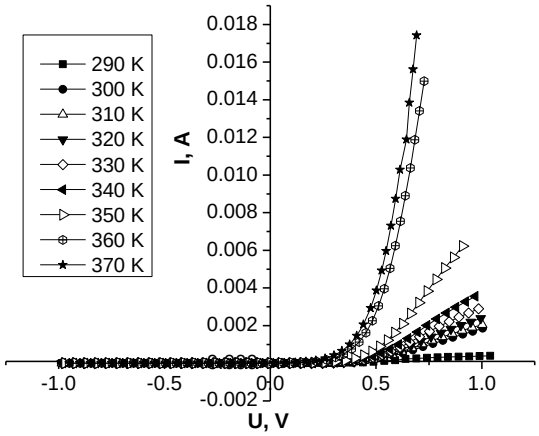

Fig. 16. Dark I-U characteristic of the poly/ITO/CdS/CdTe at various measurement temperatures, cell CS3.

The electrical parameters of this cell estimated from dark *I-U* characteristic are shown in Table 3. For the high bias the ideality factor n_2 increases linearly with the decreasing temperatures (Table 3), whereas only a slight decrease in the saturation current I_{02} is observed. At high-temperatures the diode 1 has no influence on the I-U-curves. Fig. 17 shows the semi-logarithmic forward dark I–U plots at different temperatures. We can see that the current increases exponentially with the bias voltage. At low temperatures, two different slopes at low and high biases can be observed. I–U characteristics of two diodes in the dark can be described by the expression

$$J = J_{01}[\exp q\frac{(U - JR_s)}{n_1 kT} - 1] + J_{02}[\exp q\frac{(U - IR_s)}{n_2 kT} - 1] + \frac{(U - JR_s)}{R_{sh}} \quad (12)$$

where I_{01}, I_{02} are the diode saturation currents, n_1, n_2 are the ideality factors, q is the electron charge, k is Boltzmann's constant, T is the temperature, R_s is the series resistance and R_{sh} is the shunt resistance. The first two terms of Eq. (12) describe the influences of the diodes. The different current transport mechanisms are expressed by the ideality factors and the saturation currents. The first diode with n_1 ranging from 0.9 to 1 increase slightly when rising the temperatures and expresses the diffusion process within the solar cell, the saturation current I_s decreases considerably (Fig. 18).

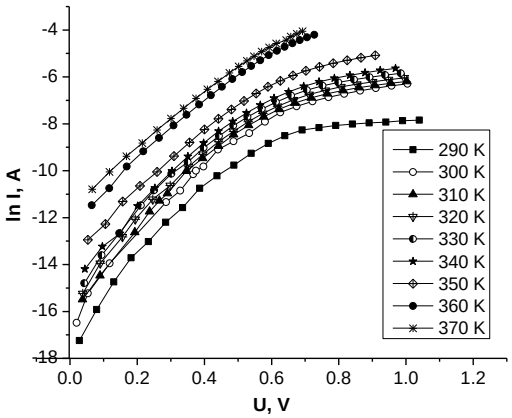

Fig. 17. Semi-logarithmic plot of forward I–V characteristics of the poly/ITO/CdS/CdTe cell at various temperatures, cell CS3.

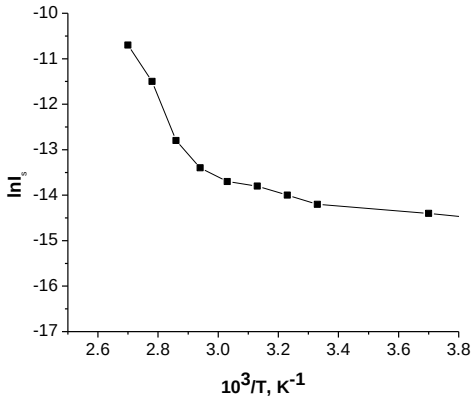

Fig. 18. Plot of ln(I_s) vs. 1/T for the poly/ITO/CdS/CdTe photovoltaic cell, cell CS3.

For the high bias the ideality factor n_2 increases linearly with decreasing temperatures (Table 3), whereas only a slight decrease in the saturation current I_{02} is observed (Fig. 18). At high-temperatures diode 1 has no influence on the *I-U*-curves. During the investigation of the dark *I-U*-curves the following has been found: up to 320 K the dark *IU*-curves could be described with the help of a two-diode model and above 320 K only with the help of a one-diode model.

3.8.Capacitance-voltage characteristics

Typical *C–U* characteristics, as a function of temperature, are presented in Fig.19. At reverse and moderately forward bias, these curves behave in the standard way, i.e. a straight Mott–Schottky ($1/C^2=f(U)$ plot is obtained. At high forward bias however, the capacitance shows one maximum and the shape of the *C–U* curves are dependent on temperature. This behavior has been found in all measured cells.

Table 3. Electrical parameters of CS3 cells at various temperatures.

T,K	1/T, K^{-1}	n	ln I_s	U_c, V
370	0,0027	2,7	-11,3	0,46
360	0,00277	2,6	-11,5	0,49
350	0,00285	2,7	-12,8	0,48
340	0,00294	2,8	-13,4	0,47
330	0,00303	2,9	-13,7	0,46
320	0,003125	3,3	-13,8	0,44
310	0,003226	3,4	-14	0,45
300	0,003333	3,5	-14,2	0,46
290	0,003448	4,1	-14,4	

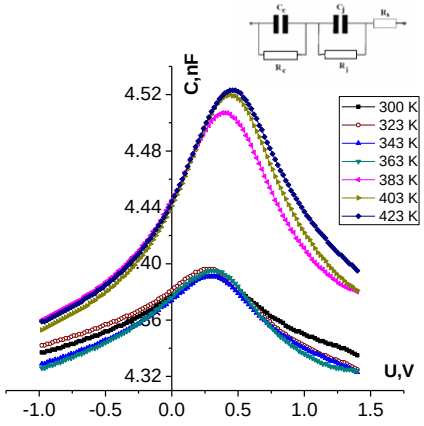

Fig. 19. The dependence of C=f (U) from the poly/ITO/CdS/CdTe cells at different temperatures, CS3.

The measurement dependencies C = f (U) at different temperatures and a frequency of 1 MHz show the typical behavior of the two-diode model. This behavior is explained as follows: at negative and moderately positive voltages (*V*~ 0.2 V), the cell junction is limiting the current, and hence the cell junction capacitance C_j is measured. At high voltages (*V*>0.2 V), the contact junction is limiting the current (causing rollover), and the contact capacitance C_c is measured. The slope of the $1/C^2=f(U)$ curve (Fig. 20) at negative and low positive voltages is determined by the CdTe doping profile in the vicinity of the CdS/CdTe junction. The slope of the $1/C^2=f(U)$ curve at a high bias is determined by the CdTe doping profile in the vicinity of the Ni/CdTe back contact.

The analysis of the $1/C^2= f (U)$ at U < 0.2 V voltages gives us the possibility to determine the effective doping concentration *N* in the CdTe layer near the solar cell junction. At the high positive bias, the effective doping concentration N_c in the CdTe layer near the back contact is calculated. The doping profiles $N(x)$ are deduced from the $1/C^2 = f(U)$ plots, and are shown in Fig. 21. The negatively and low positive voltage range (*V* <0.2V) is used to characterize the junction region; the depletion width is then the distance to the junction (at $x = 4.5$ μm) The high voltage region *U* > 0.2 V is used to characterize

the contact region; the depletion width x is then the distance to the contact (at $x = 0$). The effective doping concentration N and N_C (1-2,5) 10^{13} cm^{-3} are constant in the whole depletion width and is modified slowly with temperature.

$$x = \frac{\varepsilon_s \varepsilon_o S}{C} \qquad (13)$$

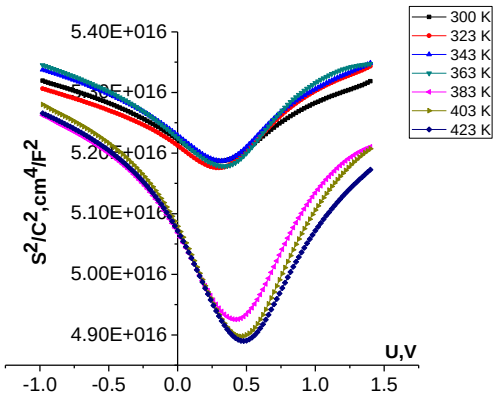

Fig. 20. The dependence of $(S/C)^2 = f(U)$ from poly/ITO/CdS/CdTe at different temperatures, CS3.

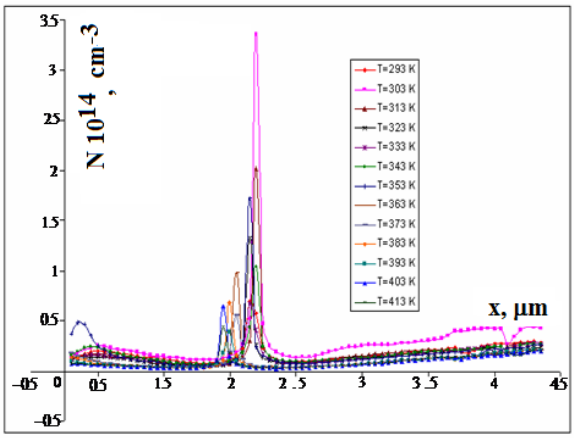

Fig. 21. Effective doping concentration (N) as a function of distance; cell CS3.

We observe from Fig. 21 that the value of the effective carrier concentration (N) in CdTe is close to 10^{15} cm^{-3} near the surface, which is about 2.25 μm away from the contact region and 2.25 - 4.4 μm away from the junction region. Thus, the CdTe layer appears to be highly doped near the surface and lowly doped between the surface and the contact and the junction regions.

4. Conclusions

The development of the superstrate ITO/CdS/CdTe photovoltaic cells on polyimide substrates is interesting, but the photovoltaic parameters are small. The current densities are low due to the light absorption in the polyimide. The open circuit voltage is low because of the lack of good ohmic contact between the CdTe layer and the Ni contact. The lack of a transparent polyimide which is stable at the high processing temperature of CdTe is a hurdle in this direction. The highest reported efficiency of a CdS/CdTe photovoltaic cell on a polyimide substrate in this paper is 4.13%. The use of very thin polyimide films and a low temperature (<400°C) process can reduce the absorption of light in the polyimide and the stability problems of the substrate.

Acknowledgments

This research was funded by EU 7th Framework Program PEOPLE International Research Staff Exchange Scheme project FLEXSOLCELLGA-2008, No. 230861.

References

[1] T. Negami, Y. Hashimoto, S. Nishiwaki, Solar Energy Materials and Solar Cells, **67**, 331 (2001).
[2] K. Ramanathan, M. A. Contreras, C. L. Perkins, S. Asher, F. S. Hasoon, J. Keane, D. Young, M. Romero, W. Metzger, R. Noufi, J. Ward, A. Duda, Prog. Photovolt: Res. Appl. **11**, 225 (2003).
[3] S. Ikegami, Solar Cells, **23**(1-2), 89 (1988).
[4] T. L. Chu, S. S. Chu, International Journal of Solar Energy, **12**(1–4), 121 (1992).
[5] C. S. Ferekides, V. Ceekala, K. M. Dugan et al., Applied Physics Letters, **67**(13), 1896 (1995).
[6] N. Romeo, A. Bosio, V. Canevari, A. Podesta Solar Energy, **77**(6), 795 (2004).
[7] Yoshihisa Tawada, Masataka Kondo, Hiroaki Okamoto, Yoshihiro Hamakawa, Solar Energy Materials **6**(3), 299 (1982).
[8] X. Wu, Solar Energy, **77**(6), 803 (2004).
[9] A. N. Tiwari, A. Romeo, D. Baetzner, H. Zogg, Progress in Photovoltaics: Research and Applications **9**(3), 211 (2001).
[10] A. Romeo, G. Khrypunov, F. Kurdesau, D. L. Bätzner, H. Zogg, A.N. Tiwari. Proceedings of the 14th International Photovoltaic Science and Engineering Conference, Bangkok, Thailand p. 715, 2004.
[11] N. Maticiuc, V. Nicorici, N. Spalatu, D. Scortescu, T. Potlog, J. Hiie, V. Valdna. Proceedings of the International Conference, CAS, 34nd Ed., Romania, **2**, 455 (2011).
[12] T. Potlog, L. Ghimpu, P. Gashin, A. Pudov, T. Nagle, J. Sites, Sol. En. Mat. & Solar Cells, **77**, 327 (2003).
[13] Singh J, Physics of Semiconductors and Their Heterostructures (McGraw-Hill), 1993.
[14] S. M. Sze, Physics of semiconductor devices (2nd edition).

*Corresponding author: tpotlog@gmail.com